A&A 375, 419–433 (2001)
DOI: 10.1051/0004-6361:20010838

Astronomy & Astrophysics

The soft X-ray eclipses of HU Aqr

A. D. Schwope[1], R. Schwarz[1], M. Sirk[2], and S. B. Howell[3]

[1] Astrophysikalisches Institut Potsdam, An der Sternwarte 16, 14482 Potsdam, Germany
[2] Space Sciences Laboratory, UC Berkeley, CA 94720, USA
[3] Planetary Science Institute, Tucson, AZ 85705, USA

Received 21 March 2001 / Accepted 7 June 2001

Abstract. We present the results of extended monitoring observations in soft X-rays of the bright eclipsing polar (AM Herculis star) HU Aqr. It was observed between 1990 and 1998 by ROSAT for a total of 230 ksec using the PSPC and the HRI detectors and by EUVE with the Deep Survey Imager and the Spectrometer for a total of 580 ksec. The overall X-ray brightness of HU Aqr varied due to changes of the mass accretion rate by a factor of 40 over that period of time. At all occasions the X-ray light curve was characterized by a marked on-off behavior due to the self-eclipse of the accreting pole. The X-ray light curve showed eclipses by the companion star, the accretion stream and by an accretion curtain raised between the two stars in the binary. Narrow dips prior to the stellar eclipse are caused by the transit of the outer accretion stream. These dips display marked phase shifts, thus indicating a large movement of the threading region, where the stream couples to the magnetic field. These shifts are shown to be related to changes of the mass accretion rate. Correspondingly, the spot longitude varied between 34° and 50°. The X-ray light curves display clear evidence for the presence of an accretion curtain, which is raised all along the ballistic accretion stream down to the region where the bulk of matter couples onto magnetic field lines. A lower limit to the mass accretion rate in the curtain is $6 \times 10^{-12}\,M_{\odot}$/yr, which is of order 10% of the total mass accretion rate. A linear fit to all available eclipse egress times yields an updated orbital ephemeris of the system: BJED$(T_0) = 2449217.345872(35) + E \times 0.086820416195(47)$ with T_0 the time of eclipse of the white dwarf centre of mass (BJED: barycentric Julian ephemeris time). The inclusion of a quadratic term gives a better fit to the data but is not regarded as indication of a period change or asynchronous rotation but by a migration of the accretion spot over the surface of the white dwarf. For one particular data set obtained in a high accretion state, detailed light curve modeling was possible. The egress from eclipse lasted 1.3 s, which constrained the azimuthal extent of the accretion spot to less than 4° or 450 km. The spot extended vertically by $\leq 0.015\,R_{\rm wd}$. A comparison of the width of the stream dip and the extent of the accretion spot shows, that only the inner 60–80% of the stream are dense enough to fire the soft X-ray engine. During the eclipse, HU Aqr was detected at a flux level of 6×10^{-14} erg cm^{-1} s^{-1}. The implied X-ray luminosity is $L_{\rm X} = 2.2 \times 10^{29}$ erg s^{-1}, comparable with X-ray emission from single, late-type, active stars.

Key words. accretion – stars: binaries: eclipsing – cataclysmic variables – stars: individual: HU Aqr – X-rays: binaries

1. Introduction

HU Aquarii is at optical and X-ray wavelengths the brightest among 12 eclipsing polars (alternatively referred to as AM Herculis stars). These consist in most cases of a main-sequence donor star and a strongly magnetic, synchronously rotating, white dwarf. The class meanwhile comprises a total of 67 systems, most of them identified as optical counterparts of soft X-ray sources.

The importance and the interest of a detailed observation of an eclipsing system is obvious. Only an eclipsing system provides an unambiguous time of reference during the orbital revolution for the study of phase-dependent phenomena and long-term changes. Thus, detailed studies of the accretion geometry, the distribution of matter in the magnetosphere, and changes in the geometry become possible.

Since its discovery as a bright source in the ROSAT-PSPC and -WFC surveys (Schwope et al. 1993, Hakala et al. 1993), HU Aqr was the target of several investigations. Glenn et al. (1994) presented optical spectroscopy

Send offprint requests to: A. D. Schwope,
e-mail: aschwope@aip.de

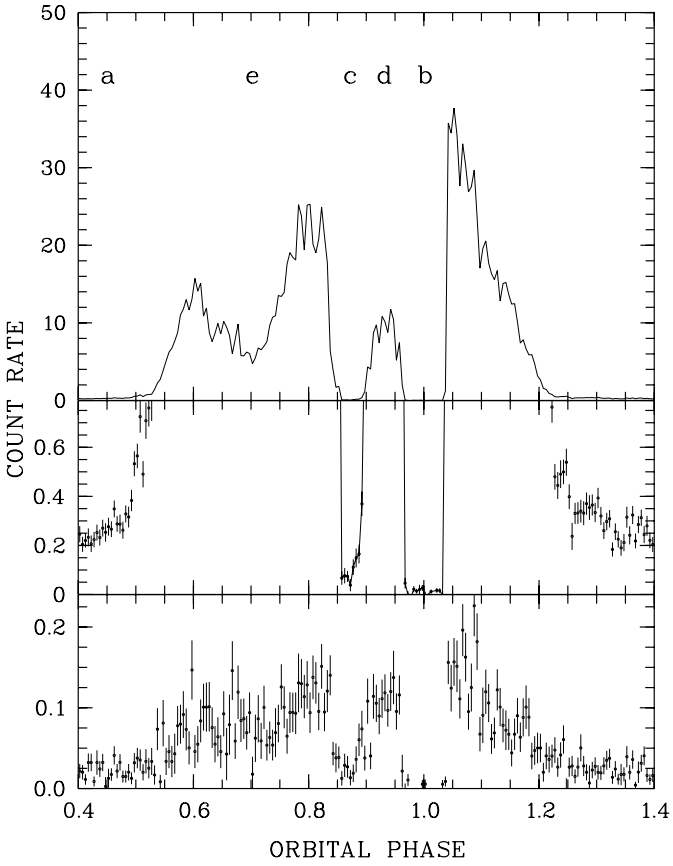

Fig. 1. ROSAT-PSPC soft X-ray light curves of HU Aqr in October/November 1993. The original data were phase-averaged using the linear eclipse ephemeris of Eq. (1). The chosen bin size is 0.005 phase units. The two upper panels show the X-ray count rate in the total ROSAT window (0.1–2.4 keV), the lower panel shows the count rate in the hard ROSAT band only (0.5–2.0 keV).

and photometry and noticed the high degree of variability of eclipse light curves indicating changes of the accretion geometry on time scales as short as hours. Hakala (1995), Harrop-Allin et al. (1999), and Vrielmann & Schwope (2001) made use of the detailed shape of optical emission line and continuum eclipse light curves in order to calculate brightness maps along the different parts of the accretion stream. Using high-resolution optical spectrophotometry analysed by Doppler tomography, Schwope et al. (1997) uncovered the existence of an extended ballistic accretion stream in HU Aqr. The high degree of asymmetry of the light curve of reprocessed line radiation from the secondary star was interpreted in terms of effective shielding by an accretion curtain.

X-ray information about HU Aqr is sparse. Schwope et al. (1993) derived an ephemeris with sufficient accuracy to extend back to the ROSAT All Sky Survey without cycle count error. They found that three of 26 scans coincided with the eclipse and found the soft part of the spectrum compatible with a blackbody of $kT_{\rm bb} \simeq 40\,{\rm eV}$. Pointed observations with the ROSAT and the EUVE satellites were numerous but so far discussed

Table 1. Log of soft X-ray observations of HU Aqr with ROSAT and EUVE (in chronological order). Given are an observation ID used in this paper, the instrument used (PSPC and HRI for ROSAT, DS/S for EUVE), the dates of observation start and end in format YYMMDD, and the total exposure time (in s).

ObsID	Detector	ObsBeg	ObsEnd	Exposure
			[s]	
P Nov. 92	PSPC	921117	921117	1522
P Apr. 93	PSPC	930423	930425	9496
P Oct. 93	PSPC	931027	931105	36716
H Apr. 94	HRI	940428	940428	5626
H May 94	HRI	940509	940514	22918
H Oct. 94	HRI	941026	941121	37189
H Nov. 95	HRI	951111	951112	26464
H Apr. 96	HRI	960424	960425	23319
D May 96	DS/S	960529	960603	125438
D Jul. 96	DS/S	960727	960730	88432
D Sep. 96	DS/S	960911	960914	78570
D Oct. 96	DS/S	961023	961028	68204
H Oct. 96	HRI	961025	961027	23348
D May 97	DS/S	970509	970514	68897
D Aug. 97	DS/S	970803	970807	84521
H May 97	HRI	970502	970514	20773
H Apr. 98	HRI	980423	980424	22438
D Aug. 98	DS/S	980827	980829	65432

Table 2. Log of optical photometry of HU Aqr. Indicated are the location and size of the telescopes (CA: Calar Alto, LS: La Silla, AIP: Potsdam), the instruments, filters ("WL" means "white light" or unfiltered observation), the total time on target and the time resolution achieved.

Date	Telescope	Instr	Filter	$T_{\rm obs}$	ΔT
				[h]	[s]
93 Aug. 16–18	CA22	MCCP	V	17.08	0.5
95 Nov. 12	LS22	EFOSC2	WL	2.34	53
96 Jul. 19–21	AIP07	CCD	WL	5.14	12
96 Sep. 1–5	AIP07	CCD	WL	10.90	12
98 Sep. 24	AIP07	CCD	V	1.84	12

mainly in thesis works or conference proceedings (Sohl et al. 1995; Sohl 1997; Schwope 1995; Schwope 1996; Schwope et al. 1998; Sirk & Howell 1998). In these papers, notions about the occurrence of stream dips and an accretion curtain based on X-ray data are given. Here we present the synopsis and analysis of all observations performed at soft X-ray wavelengths with ROSAT and EUVE. The paper is organized in the following way. In Sect. 2 we describe the data sets which were subsequently analysed in this work. General remarks on the variable shape of the soft X-ray light curves are made in Sect. 3. The eclipse is studied in Sect. 4, where the eclipse ephemeris, the eclipse egress and the residual flux in the eclipse are analysed. A spectral analysis is carried

out in Sect. 5. The narrow absorption dips and the density of the accretion stream are addressed in Sect. 6. Our main results are summarized and discussed in context in Sect. 7.

2. Observations and reductions

An overview of the soft X-ray observations of HU Aqr is given in Table 1. The table lists only pointed observations, the ROSAT All Sky Survey observations were described in Schwope et al. (1993), the source was not seen in the EUVE All Sky Survey (Bowyer et al. 1996) where the region of HU Aqr received an exposure of 935 s with the Lexan filter. The 3σ upper limit count rate in the EUVE survey is $0.05\,\mathrm{s}^{-1}$.

Table 1 lists the information about an observation ID used in this paper, the X-ray detector, the date of the observation, and the total exposure time.

At two occasions (Oct. 96, May 97) we could arrange simultaneous observations with both the ROSAT and the EUVE satellites. The corresponding light curves are discussed in the Sect. 3, the implications for the X-ray spectral shape in Sect. 5.

The region of HU Aqr was exposed for a total of 48 ksec with the ROSAT-PSPC, for 182 ksec with the ROSAT-HRI, and for 579 ksec with the DS/S instruments on board EUVE, respectively. The source was always positioned on-axis, hence, some variability in the PSPC observations might be apparent only due to blocking of X-ray photons by the wire-mesh of the entrance window of the detector. Source photons were extracted from the original photon event tables, background and vignetting corrected using MIDAS/EXSAS (Zimmermann et al. 1994) and IRAF software packages. Binned light curves (see Fig. 2) were computed using the ephemeris given in Eq. (1).

For the high-state ROSAT-PSPC observations in October/November 1993 we also determined hardness ratios HR1 and SR as a function of orbital phase which characterize spectral variations. The hardness ratio HR1 is determined in the usual manner, $\mathrm{HR1} = (H - S)/(H + S)$, with H and S the counts in the hard (0.5−2.0) keV and soft ROSAT (0.1−0.4) keV bands, respectively. Fortunately, in polars the two bands are sensitive to the two main radiation components usually encountered in these systems. H is sensitive to radiation from the hot post-shock cooling plasma (well approximated as a bremsstrahlung spectrum at ROSAT resolution), and S is sensitive to the soft component of reprocessed radiation from the heated stellar photosphere (at ROSAT resolution reasonably well approximated as a blackbody spectrum). Hence, HR1 is a measure of the relative weight between these two main spectral components. Variations of HR1 can be caused by a variable column density, which in the first place affects the counts in the soft band, or by intrinsic changes of the spectral parameters.

The hardness ratio SR is a hardness ratio built in the soft component, $\mathrm{SR} = (S1 - S2)/(S1 + S2)$, with $S1$ and $S2$ being the counts in the soft sub-bands ($S1 = (0.30\text{–}0.50)\,\mathrm{keV}$, $S2 = (0.1\text{–}0.30)\,\mathrm{keV}$). The hardness ratio SR is sensitive to variations of either kT_{bb} or N_{H}.

Contemporaneous optical photometric observations were performed in 1993, 1995, 1996 and 1998 using high-speed photometers and CCD cameras mounted to telescopes at La Silla, Calar Alto and the AIP 70 cm telescope. The latter provided the largest database. Details of the observations are given in Table 2 and the phase-averaged light curves are shown in Fig. 3. All data are shown twice for clarity, the detected counts of HU Aqr were related to those of the $V = 14\overset{\mathrm{m}}{.}7$ comparison "C" in the chart of Schwope et al. (1993).

3. Soft X-ray and optical light curves of HU Aqr

3.1. Main characteristics of the soft X-ray light curves

We start the analysis with a description of the main observed features of the X-ray light curves of HU Aqr, using as an example the ROSAT-PSPC observation obtained in October/November 1993 (Fig. 1, top panel). In the different panels of Fig. 1 we show (from top to bottom) (i) the X-ray light curve in the full ROSAT-band, (ii) the same on an expanded y-scale, and (iii) the light curve in the hard passband only. The spectral variability may be obtained from phase-dependent hardness ratio curves shown in Fig. 10.

The light curve shows five main characteristics described subsequently, labeled *a*–*e* in the top panel of Fig. 1.

(a) The light curve has a clear on-off pattern caused by the self-eclipse of the accretion spot by the white dwarf. The difference between bright phase centre and eclipse centre yields the azimuth (longitude) of the main accretion spot with respect to the line joining both stars. The length of the X-ray bright phase depends on the orbital inclination, the latitude of the spot (measured with respect to the rotation axis, referred to as co-latitude), as well as its vertical and longitudinal extent. Characteristic parameters of the light curves (the mean bright-phase count rate, the centre of the bright phase, the phase of eclipse egress and the phases of narrow and broad dips) obtained at different epochs are listed in Table 3. During the faint phase, when the accretion spot is self-eclipsed, X-rays are not switched off completely. The minimum faint-phase PSPC count rate in Oct. 1993 was $\sim 0.25\ \mathrm{s}^{-1}$. Maximum count-rate in the bright phase was observed at phase 0.05, it reached $\sim 40\,\mathrm{s}^{-1}$ in the phase-averaged light curve with 200 phase bins. Using bins of 0.25 s width, the rate reached $145\,\mathrm{s}^{-1}$. Emission during the bright phase is super-soft with HR1 near to −1.0, during the faint phase a slight spectral hardening is observed, but the hardness ratio HR1 $\simeq -0.8$ indicates still very soft emission.

The X-ray bright phase is markedly modulated by the stellar eclipse *(b)*, a narrow dip *(c)*, and a broad dip *(e)*.

(b) The feature at phase 0.0 is the eclipse of the accretion region by the secondary star. This is not exactly coincident with the eclipse of the white dwarf itself.

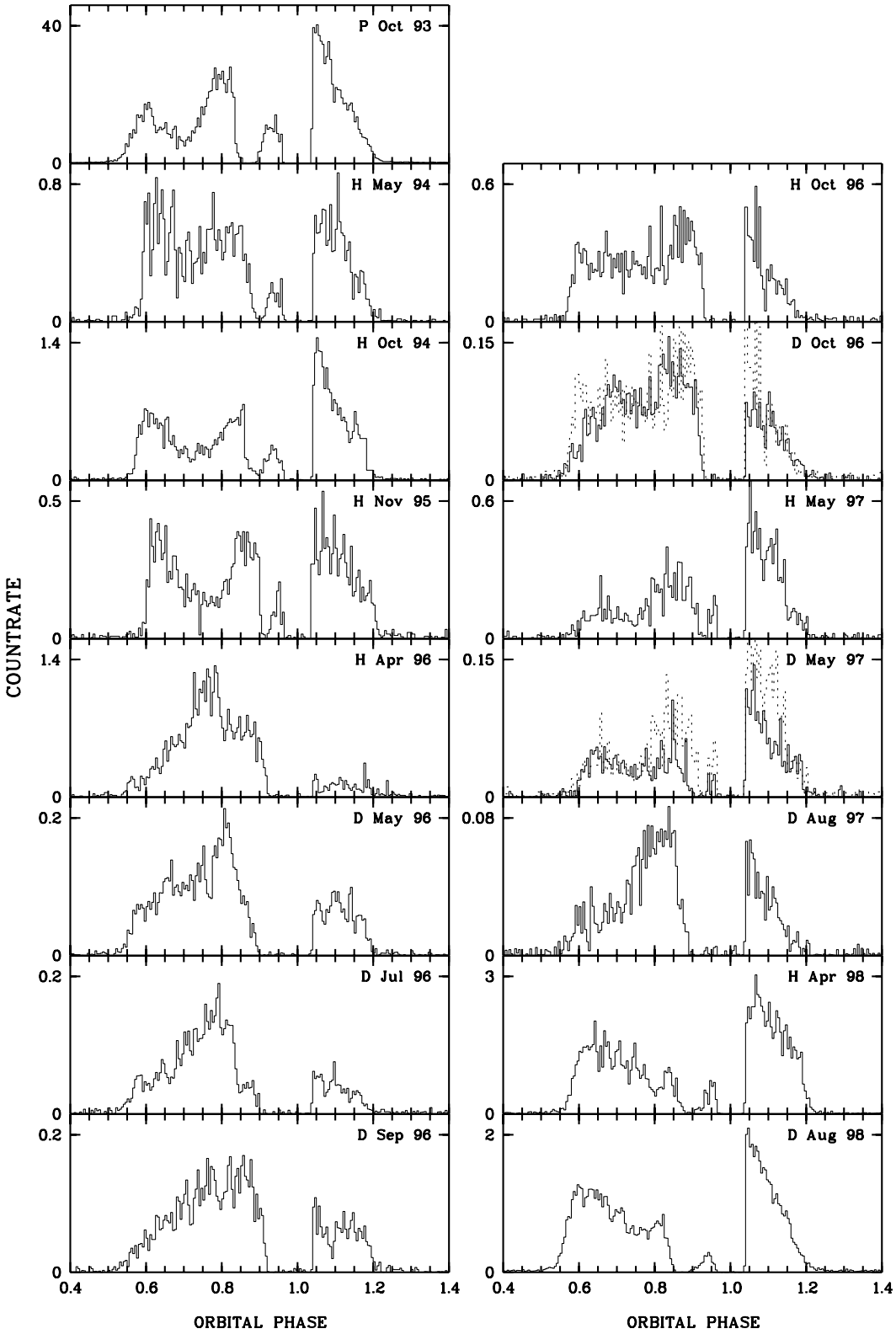

Fig. 2. Collection of ROSAT and EUVE soft X-ray light curves of HU Aqr obtained between 1993 and 1998 in chronological order. These light curves are only for observations covering an entire orbital cycle. The letter before the date printed in each panel indicates the satellite/detector combination: P – ROSAT PSPC, H – ROSAT HRI, D – EUVE DSS. All data were phase-averaged according to the ephemeris of Eq. (1), the bin size is 0.005 phase units. The dotted lines in the panels of the "D OCT. 96" and "D MAY 97" EUVE-observations are the scaled, quasi-simultaneous HRI-light curves.

The phase offset is caused by an offset of the accretion spot with respect to the line joining both stars (azimuth of the spot is not equal zero).

(c) The originally free-falling accretion stream becomes dominated by the magnetic field and threadened at some location in the binary system (see Fig. 9 and also Schwope et al. 1997 for a sketch of the accretion geometry of HU Aqr). Following magnetic field lines, the stream is lifted out of the orbital plane. If the accretion pole and the observer are located in the same hemisphere of the binary (with respect to the orbital plane), an absorption dip occurs when the line of sight crosses the accretion stream. In a high inclination system like HU Aqr the measured azimuth of the dip centre equals the azimuth of the threading region. The observed width of the dip indicates the azimuthal extent of the threading region. Since soft X-rays are more affected by photoelectric absorption than hard X-rays, the hardness ratios HR1 and SR increase at dip phase (see Sect. 6). We note, that a similar re-emergence of (softer) X-rays after the dip, and before the eclipse, also occurs in MN Hya (Buckley et al. 1998).

(d) Compared to the pre-dip and the post-eclipse count rate the X-ray flux is clearly reduced between the narrow dip and the eclipse. At the same time the hardness ratios SR and HR1 indicate a spectral hardening. Both, the flux decrease and the spectral change are suggestive of enhanced absorption in an accretion curtain, which is raised all along the ballistic stream between L_1 and the narrow dip, where most of the matter couples onto field lines. An $N_{\rm H}$-map of the dip and the curtain is presented in Sect. 6.

(e) A broad dip centred on phase 0.7, i.e. after the phase of initial rise, is evident in the light curve shown in Fig. 1. A similar light curve in general and a similar dip feature in particular was observed in UZ For (Warren et al. 1995; Sirk & Howell 1998). These authors concluded, that the observed width of the dip suggests that light is being removed from the line of sight by material close to the point of origin, i.e. X-rays are absorbed or scattered in the accretion column just above the accretion spot. We address this interpretation with the aid of an $N_{\rm H}$-map in Sect. 6.

3.2. Evolution of the soft X-ray light curve

A montage of all available soft X-ray light curves with full phase coverage obtained during pointed ROSAT and EUVE observations is shown in Fig. 2. This collection shows the strong evolution of the soft X-ray light curve of HU Aqr. The preserved features are the on-off behavior due to the self-eclipse of the accretion spot and the stellar eclipse at phase zero. The X-ray brightness, the offset between centre bright phase and eclipse centre, the occurrence of the broad dip, the phase of the narrow dip and the size of the accretion curtain, however, are subject to marked changes. We describe here the most prominent changes and list characteristic phases and count-rates extracted from the phase-folded light curves in Table 3.

In October 1996 and May 1997 we could arrange truly simultaneous observations with ROSAT and EUVE for a total of about 4950 s and 3140 s, respectively, split in several OBIs. The typical length of a simultaneous observation was about 500–600 s. The average count rate ratio HRI/DS, determined for data intervals with EUVE count rate above 0.05 $\rm s^{-1}$, is 2.2 with a standard deviation of 0.8. The ratio of the overall light curves at the two occasions seems to be better reflected by a factor ≥ 3. The ratio becomes as large as 6 in the post-eclipse interval of the May 1997 observation. For comparison, we plotted the scaled HRI light curves (scaled with a factor of 3) as dotted lines in the corresponding panels of the EUVE light curves in Fig. 2. This large scatter reflects the high intrinsic variability of the source on a time scale as short as days or even orbital cycles. The high degree of variability becomes obvious also from the rather densely spaced EUVE-monitoring observations in 1996, which took place every one or two month. Throughout this paper we will use a HRI/DS conversion factor of 2.2.

In Table 3 we quote the count rates measured directly in the light curves and equivalent (or scaled) HRI count rates (prefix 'S'). These were derived from the observed rates using count conversion factors HRI/DS = 2.2 and PSPC/HRI = 8.0. The HRI/DS conversion is based on intervals of simultaneous observation, the PSPC/HRI conversion factor is based on folding the best-fit two-component spectrum of the 1993 PSPC-observation through the spectral response of the two detectors (see Sect. 5).

In order to characterize the X-ray brightness at each occasion, we list in Table 3 a mean peak count rate, $\rm CR_m$, and the mean count rate in the phase interval 0.05–0.10, $\rm CR_1$. The mean peak count rate is measured in the brightest contiguous 10% phase interval of the light curve. The scaled, post-eclipse count rate varies by a factor of > 40 reaching a maximum of $4.4\,\rm s^{-1}$ in "P Nov. 93". The average faint-phase count rate, $\rm CR_f$, was as high as $0.3\,\rm s^{-1}$, but in most cases was near the detection limit or below.

Even in the phase-averaged light curves strong X-ray flares can be easily recognized. These may stick out by factors up to $\sim$10 above the average count rate and are explained as caused by accretion events.

One prominent change of the light-curve shape is related to the narrow dip and absorption in the accretion curtain. The narrow dip displays a clear motion in phase (noted earlier by Glenn et al. 1994; Schwope 1996; Harrop-Allin et al. 1999 in optical or combined X-ray/optical data) and migrates towards the eclipse during episodes of reduced X-ray brightness. At times, the narrow dip is completely merged with the eclipse. Again, this special appearance became most obvious in 1996, when the accretion rate was at the lower limit of the range observed by us. We measured the phase of the narrow dip as phase of half intensity during ingress to the dip (which is possible for all occasions) as well as its centre phase, when the

dip showed an ingress and an egress. The results are listed in Table 3, plotted in Fig. 8 and discussed in more detail in Sect 6.

A second change is related to ingress from and egress into the self-eclipse, which is occasionally rather steep (e.g. "H May 94", "H Nov. 95") and sometimes very shallow (e.g. "H Apr. 96", "D Sep. 96"). These features are related to a restructuring of the extent of the accretion region.

A third prominent change is the (apparent) absence of the broad dip in almost all 1996 observations and in "D Aug. 97". In the light curve of the latter observation at least a flux depression can be recognized at phase 0.7. Light curves without broad dip have the phase of maximum count rate in the centre of the bright phase. When the broad dip is clearly present in the light curve, maximum emission occurs in the phase interval 0.05–0.10, i.e immediately after eclipse. Interestingly, the broad dip recovers when the system returns to high count rates, its existence thus seems to be correlated with the accretion rate.

3.3. Contemporaneous optical photometry

Optical photometry was obtained on several occasions during recent years thus supporting our X-ray observations. The separation between X-ray and optical observations ranges from one day only (Nov. 12, 1995) to about two months (Aug. 1993). Given the high degree of variability of HU Aqr observations of the latter kind can be regarded only as suggestive of the probable optical state at the time of the X-ray observation. The phase-averaged optical light curves obtained at five different epochs are shown in Fig. 3.

HU Aqr was in a high accretion state during the RASS, and also during pointed ROSAT observations in 1992 and 1993. The system then entered an extended state of reduced accretion and reappeared at a high brightness level in 1998, $V_{\rm max} \simeq 14\overset{\rm m}{.}5$. As described in Schwope et al. (1993), the system faded optically by 1.5 mag during the four nights of observation in late September 1992. During the EUVE all-sky survey in November 1992 it was in a low state.

In the high states the optical light curves are double-humped, likely due to strong cyclotron beaming, with a maximum brightness of $V = 14\overset{\rm m}{.}5$. In our high-state observations at two epochs (1993 and 1998), a pronounced optical pre-eclipse absorption dip can be recognized. Orbital variability outside eclipse and dip was between $V = 14\overset{\rm m}{.}7-15\overset{\rm m}{.}1$ in 1993, and between $V = 14\overset{\rm m}{.}5-14\overset{\rm m}{.}8$ in 1998. The dip was centred at $\phi = 0.86$ in 1998, and at $\phi = 0.88$ in 1993, i.e. it occurred earlier in phase when the system was brighter.

At reduced brightness (=accretion rate) in 1995 and 1996 no pre-eclipse dip is observed. The shape of the light curve is then more or less single-humped with orbital variability outside eclipse between $V = 16\overset{\rm m}{.}1-16\overset{\rm m}{.}7$ in July 1996, and $V = 16\overset{\rm m}{.}3-17\overset{\rm m}{.}0$ in September 1996. Strong, 0.5 mag, flaring activity occurs during the bright phase.

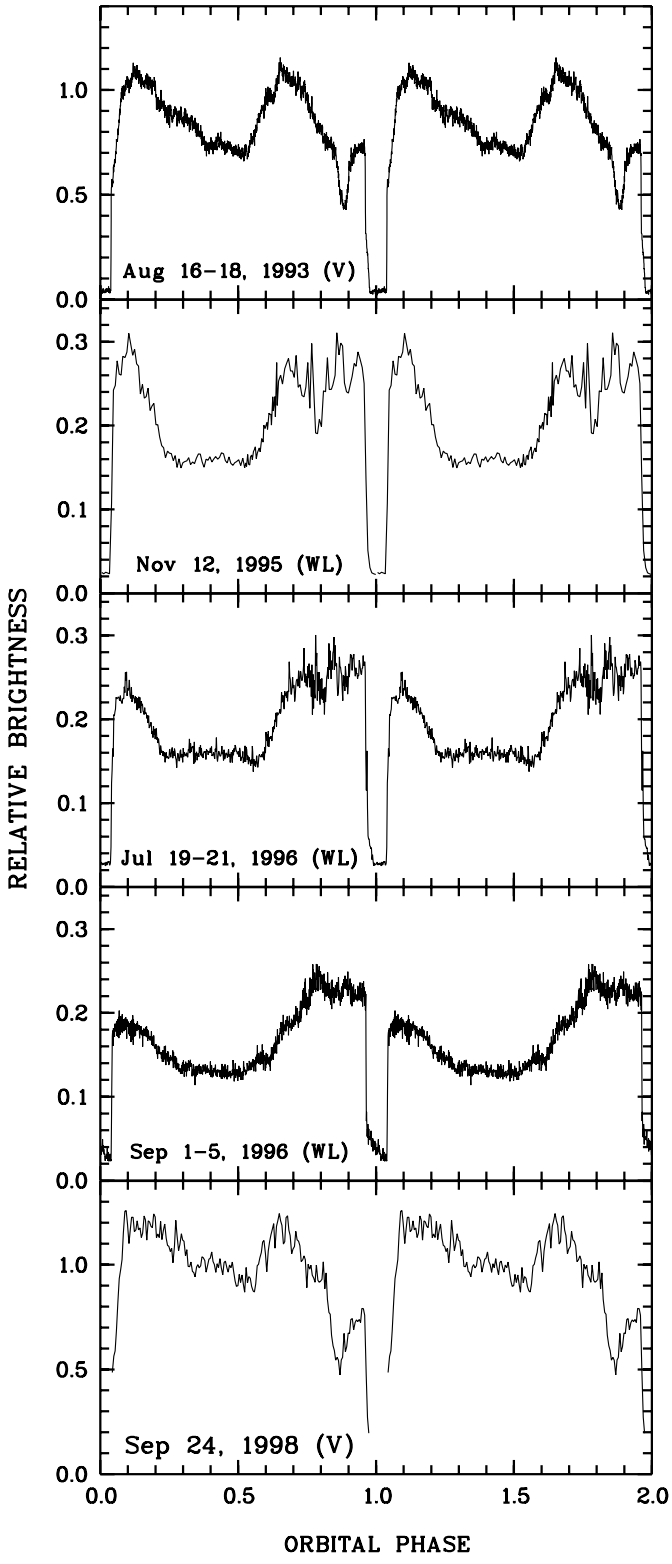

Fig. 3. Results of optical photometric observations performed in parallel to the X-ray observations. The light curves were phase-averaged and normalized to the counts of the $V = 14.7^{\rm m}$ companion star.

Table 3. Characteristic features of the phase-averaged soft X-ray light curves of HU Aqr. Columns 1 and 2 give the modified Julian date at start and end of the observation. Column 3 gives the approximate date, Col. 4 identifies the instrument used (S: EUVE All Sky Scanner Survey, P: ROSAT PSPC, H: ROSAT HRI, D: EUVE Deep Survey Imager). Columns 5–8 indicate the phases of the bright phase centre $\phi_{\rm CB}$, the phase of narrow dip ingress (half intensity at ingress) $\phi_{\rm DH}$, the phase of the narrow dip centre $\phi_{\rm DC}$, and the phase of the broad dip centre $\phi_{\rm BD}$. $\rm CR_m$, $\rm CR_1$, and $\rm CR_f$ are the count rates at peak, in the phase interval 0.05−0.10, and in the faint phase, $\Delta\phi = 0.30-0.45$, respectively (Cols. 9–11). Columns 12 and 13 list the count rates scaled to the HRI. The PSPC/HRI conversion factor was 8.0, the HRI/DS conversion factor was 2.2. For values given in Cols. 5–7, the typical phase uncertainty is 0.003 phase units. Values with larger uncertainties are marked with a colon. For values given in Col. 8, the typical phase uncertainty is 0.03 phase units. In Col. 11 values in parentheses indicate the uncertainty in the last digits quoted.

(1) MJD1	(2) MJD2	(3) Date	(4) Inst	(5) $\phi_{\rm CB}$	(6) $\phi_{\rm DH}$	(7) $\phi_{\rm DC}$	(8) $\phi_{\rm BD}$	(9) $\rm CR_m$	(10) $\rm CR_1$	(11) $\rm CR_f$	(12) $\rm SCR_m$	(13) $\rm SCR_1$
48933.500	48938.799	Nov. 92	S	–	–	–	–	$<0.05^a$	$<0.05^a$	–	–	
48944.478	48944.496	Nov. 92	P	–	–	–	–	$:0.6^b$	–	–	–	–
49101.069	49102.996	Apr. 93	P	–	–	–	–	5.0	4.29	0.053(36)	0.63	0.54
49288.200	49291.273	Oct. 93a	P	0.874	0.828	0.873	–	22	–	0.314(75)	2.8	–
49294.895	49295.438	Nov. 93b	P	–	0.839	0.868	0.70	38	29.5	0.267(76)	4.8	3.7
49295.825	49296.571	Nov. 93c	P	0.871	0.837	0.872	0.73	30	35.3	0.29(13)	3.8	4.4
49471.181	49471.331	Apr. 94	H	0.888	0.910	0.926	0.76	–	–	–	–	–
49482.061	49487.322	May 94	H	0.890	0.878	0.900	0.77	0.65	0.53	0.003(9)	0.65	0.53
49652.251	49677.970	Oct. 94	H	0.881	0.861	0.892	0.75	0.9	1.08	0.005(10)	0.9	1.08
50032.550	50033.840	Nov. 95	H	0.902	0.901	0.918	0.77	0.35	0.34	0.004(10)	0.35	0.34
50197.529	50199.337	Apr. 96	H	0.870	0.913	–	–	1.0	0.12	0.006(10)	1.0	0.12
50232.606	50237.676	May 96	D	0.868	0.875:	–	–	0.14	0.069	0.001(2)	0.31	0.15
50291.710	50294.624	Jul. 96	D	0.862	0.900	–	–	0.13	0.049	0.001(3)	0.29	0.11
50337.812	50340.851	Sep. 96	D	0.873	0.913	–	–	0.14	0.061	0.001(3)	0.31	0.13
50382.315	50384.446	Oct. 96	H	0.869	0.929	–	0.74	0.38	0.32	0.004(12)	0.38	0.32
50382.318	50384.500	Oct. 96	D	0.880	0.922	–	0.77	0.15	0.070	0.000(3)	0.33	0.15
50570.639	50582.925	May 97	H	0.895	0.916	0.929	0.75	0.63	0.43	0.004(12)	0.63	0.43
50577.724	50582.930	May 97	D	0.905	0.895	0.916	0.76	0.087	0.094	0.000(2)	0.19	0.21
50664.298	50667.604	Aug. 97	D	0.874	0.873:	0.910:	0.69	0.064	0.045	0.001(2)	0.14	0.10
50927.077	50928.420	Apr. 98	H	0.889	0.862	0.898	–	2.2	2.31	0.014(9)	2.2	2.31
51053.405	51055.396	Aug. 98	D	0.875	0.840	0.880:	0.74	1.45	1.71	0.022(9)	3.2	3.76

[a] 3σ upper limit.
[b] Incomplete phase coverage.

Large differences are observed during the eclipses at different occasions. After the initial steep ingress due to eclipse of the white dwarf a phase of slower decrease of brightness follows. This decrease of brightness is due to the eclipse of the accretion stream. This event may last only about two minutes (Aug. 93, top panel of Fig. 3) or even as long as 8−10 min (Sep. 96). The observed large differences indicate a remarkable re-arrangement of the stream in the magnetosphere of the white dwarf. The general trend is that a high state corresponds to a short ingress of the stream and a low state to a long ingress. This is certainly contrary to the expectation, since in the high accretion state the ballistic stream is much longer than in the low accretion state. The reason for this discrepancy is unknown presently and will be investigated separately in a dedicated paper.

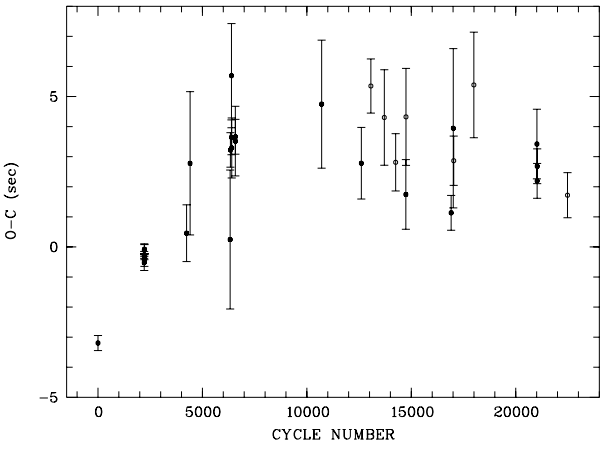

Fig. 4. Observed minus calculated times of eclipse egress of HU Aqr with respect to a linear ephemeris. Open symbols represent EUVE data, filled symbols represent ROSAT-data.

4. The X-ray eclipse of HU Aqr

4.1. The X-ray eclipse ephemeris

Although the phase of eclipse ingress was covered several times during our observations, it is clearly resolved only in a few cases. At this binary phase the accretion curtain absorbs most of the X-ray photons, hence we are lacking photons for a precise determination of eclipse ingress. For the determination of the orbital period from X-ray data

Table 4. X-ray eclipse egress times of HU Aqr and their corresponding orbital phases with respect to Eq. (1). BJED is the barycentrically corrected ephemeris time of the eclipse egress.

Cycle	BJED	ΔBJED	$\phi_{\rm orb}$
	2 440 000+		
0	9102.9200026	0.0000029	0.039612
2212	9294.9667944	0.0000013	0.039972
2213	9295.0536119	0.0000031	0.039938
2216	9295.3140780	0.0000024	0.039993
2222	9295.8349966	0.0000024	0.039948
2225	9296.0954591	0.0000012	0.039964
2226	9296.1822824	0.0000018	0.039997
4241	9471.1254248	0.0000109	0.040010
4409	9485.7112814	0.0000276	0.040347
6328	9652.3196284	0.0000267	0.039982
6341	9653.4483283	0.0000066	0.040379
6390	9657.7025335	0.0000067	0.040435
6391	9657.7893776	0.0000200	0.040708
6403	9658.8311948	0.0000115	0.040387
6576	9673.8511292	0.0000134	0.040415
6579	9674.1115921	0.0000067	0.040434
10707	10032.5062777	0.0000246	0.040521
12607	10197.4650434	0.0000138	0.040233
13064	10237.1420028	0.0000104	0.040568
13707	10292.9675175	0.0000184	0.040420
14250	10340.1109856	0.0000110	0.040214
14740	10382.6529766	0.0000134	0.040065
14746	10383.1739289	0.0000187	0.040408
16906	10570.7059884	0.0000067	0.039953
17010	10579.7353441	0.0000306	0.040326
17030	10581.4717399	0.0000095	0.040182
17994	10665.1666491	0.0000203	0.040504
21014	10927.3642796	0.0000134	0.040200
21023	10928.1456491	0.0000067	0.040037
21026	10928.4061160	0.0000067	0.040101
22478	11054.4693474	0.0000087	0.039953

alone we make use of the frequently covered eclipse egress, which is not affected by absorption in the binary itself. The time of eclipse egress was determined using two different approaches, depending on the brightness of the target. All egress times with their errors are collected in Table 4, the times quoted there are corrected for the solar system barycentre and account for the leap seconds introduced during recent years (barycentric Julian ephemeris time, BJED).

If the source was sufficiently bright, eclipse egress was defined as the arrival time of the second photon at the expected egress time in the original photon event table (PET). The uncertainty given in Table 4 is then the rms of the first three photons. If the source was faint, $<1\,{\rm s}^{-1}$, the original PET was phase-folded and time-binned. The times quoted for these observations in Table 4 are the times of those bins marking the end of the eclipse. The errors given in the table correspond to the bin width.

A weighted linear regression to all times collected in Table 4 yields the ephemeris $T_0 = 2449102.920033366(73) + E \times 0.086820416195(47)$ with a reduced $\chi^2 = 10.8$. The diagram in Fig. 4 compares the observed and calculated times of egress. It shows systematic deviations from a linear trend. A quadratic ephemeris BJED $= T_0 + EP + \frac{1}{2}P\dot{P}E^2$ with $T_0 = 2449102.920011942(73)$, $P = 0\overset{\rm d}{.}086820426745(47)$ and $\frac{1}{2}P\dot{P} = -43(3) \times 10^{-14}$ days yields a significantly smaller reduced χ^2 of 2.6 (values in parenthesis give formal statistical errors). This finding can be regarded either as an indication of a true period change, or as an indication of an asynchronously rotating white dwarf or as migration of the accretion spot, probably in response to accretion rate changes. We favor the latter interpretation, since also the phasing of the bright phase changes in response to accretion rate variations (see Sect. 6) and because the largest changes are observed on a very short time-scale between April and October 1993. The implications of this interpretation are further discussed and modeled in Sect. 4.3. All phases in this paper refer to the linear ephemeris given in Eq. (1)

$$\begin{aligned}{\rm BJED}(T_0) \;&=\; 2449217.345872(35)\\ &\quad +E \times 0.086820416195(47). \end{aligned} \qquad (1)$$

The error of the period quoted in parentheses is the formal statistical error of our linear fit to the ROSAT/EUVE-timings. The time T_0 is the time of superior conjunction of the white dwarf centre of mass, determined by high-time resolution HST/FOS and observations optical high-speed photometry (Schwope et al., in preparation). The systematic uncertainty of the HST-based zero point of the ephemeris is 3 s, also quoted in parenthesis. In order to convert times given as BJED to barycentric Julian dates (BJD) one has to subtract the accumulated number of leap seconds = 60.184 s. The zeropoint given in BJD is 2449217.345176(35).

4.2. Eclipse emission – X-ray's from the secondary star

Secondaries in CVs are rapidly rotating, late-type stars. Pronounced magnetic activity accompanied by emission of coronal X-rays may therefore be expected. Compared to the typical accretion luminosity of $10^{32} \ldots 10^{33}\,{\rm erg\ s^{-1}}$ coronal emission of the order of $10^{29}\,{\rm erg\ s^{-1}}$ is almost negligible and extremely difficult to detect. This is particularly true for the majority of the systems which are non-eclipsing. The 9 eclipses of HU Aqr covered during the two PSPC pointings in 1993 provide the unique opportunity to directly access the secondary in a CV at X-ray wavelengths.

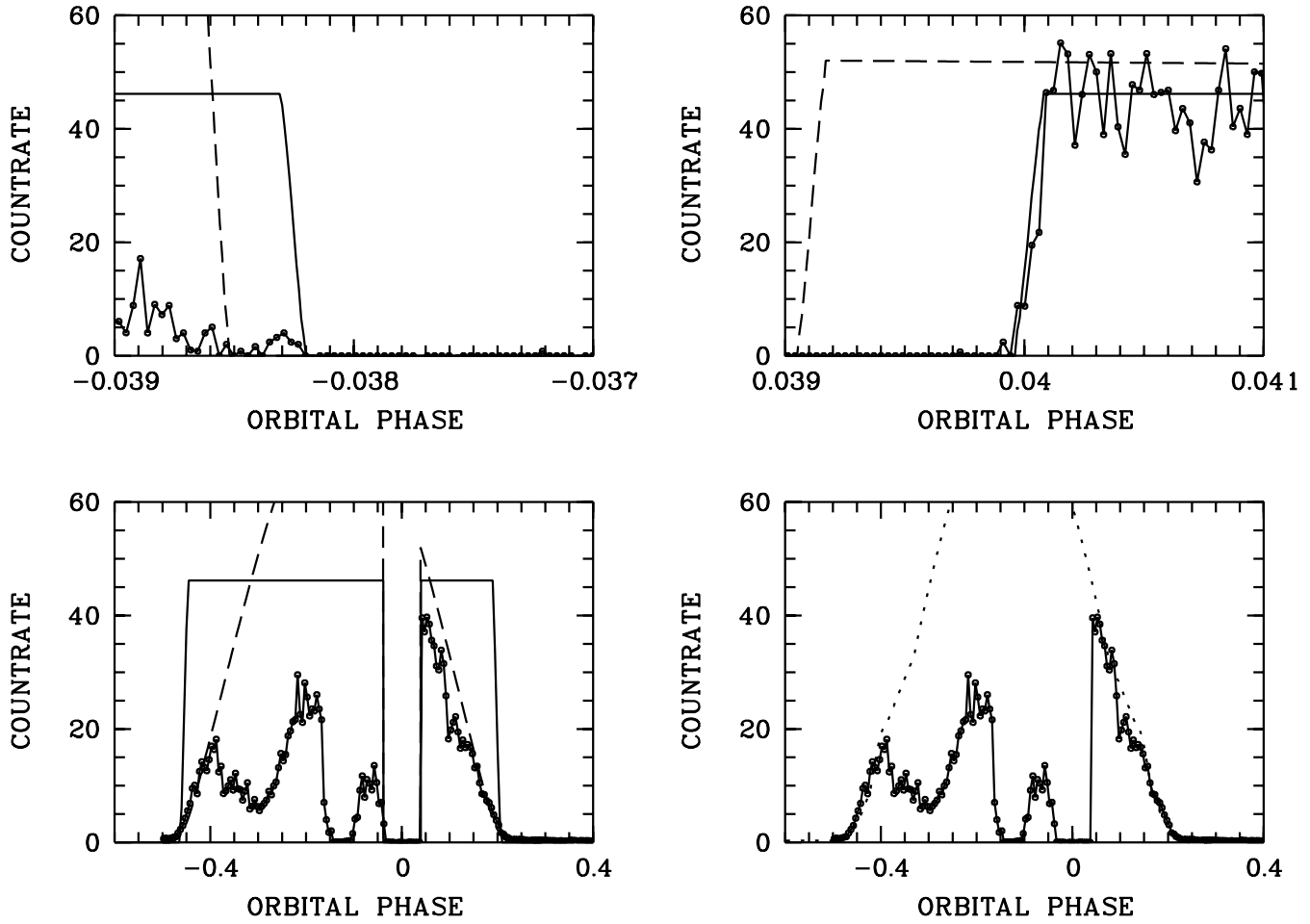

Fig. 5. Comparison of model light curves with PSPC 93 observations of HU Aqr. Small circles connected with polygons are the phase-folded PSPC-data. The dashed line is a model fit for an accretion spot without vertical extent with foreshortening factor, the solid line is a fit with vertical extent, $h = 0.015\,R_{\rm wd}$, and without foreshortening factor. The top panels are centred on eclipse ingress and egress, the time interval along the abscissa is 15 s only, one tick corresponds to 0.75 s. The dotted line in the lower right panel is the result of a fit with the 3D model.

Sohl et al. (1996) claimed a positive X-ray detection of HU Aqr during eclipse at a count rate of $0.018\,{\rm s}^{-1}$ from the Oct./Nov. 1993 data alone. Using the same data set, we find no X-ray source with an existence likelihood ML > 5, (ML $= -\ln(p)$, with p being the probability that a source is the result of a statistical fluctuation). After inclusion of the April 1993 dataset the total exposure during eclipse, $\phi = 0.97{-}1.03$, was 3080 s. Within the specified phase interval 20 photons were collected at the position of HU Aqr, giving a maximum likelihood of existence of an X-ray source at that position of 9. This corresponds to a vignetting and dead-time corrected count rate of 0.007 ± 0.002 cts s^{-1}, a factor of 3 lower than Sohl's estimate.

After ingress of the white dwarf at phase $\phi = 0.962$ parts of the accretion stream are still visible and detected in the optical light curves. The stream eclipse is total only at $\phi = 0.98$. The stream could be a source of X-rays, e.g. due to scattering or internally due to shock heating. If so, we would expect more photons during first part of the eclipse. This is not obviously the case but the limited statistics of our detection does not permit any secure statement. For the time being we assume that all photons detected during the eclipse are originating from the secondary star in HU Aqr.

The X-ray flux of the secondary at Earth is 5.8×10^{-14} ergs s^{-1} cm^{-2} using the count-energy conversion ECF $= (5.30 \times {\rm HR1} + 8.31)\ 10^{-12}$ erg cm^{-2} cts^{-1} derived by Schmitt et al. (1994) based on a study of a complete sample of main-sequence stars. At the likely distance to HU Aqr of 180 pc, the red star's luminosity is 2.2×10^{29} ergs s^{-1}. The luminosity of an adopted M5 main sequence secondary is $\log(L/L_\odot) = -2.1$. With our measured X-ray luminosity $L_{\rm X}$ the ratio $L_{\rm X}/L_{\rm bol}$ for the secondary in HU Aqr is $L_{\rm X}/L_{\rm bol} = 0.007$ ($\log(L_{\rm X}/L_{\rm bol}) = -2.2$). Information about X-ray luminosities (in absolute and relative units) of single stars at the bottom of the main sequence is sparse. ROSAT studies of several young open clusters by Prosser et al. (1996, 1998) show, that our measured eclipse X-ray flux is in full agreement with those of late-type stars in the clusters. Particularly interesting is the increase of $\log(L_{\rm X}/L_{\rm bol})$ for

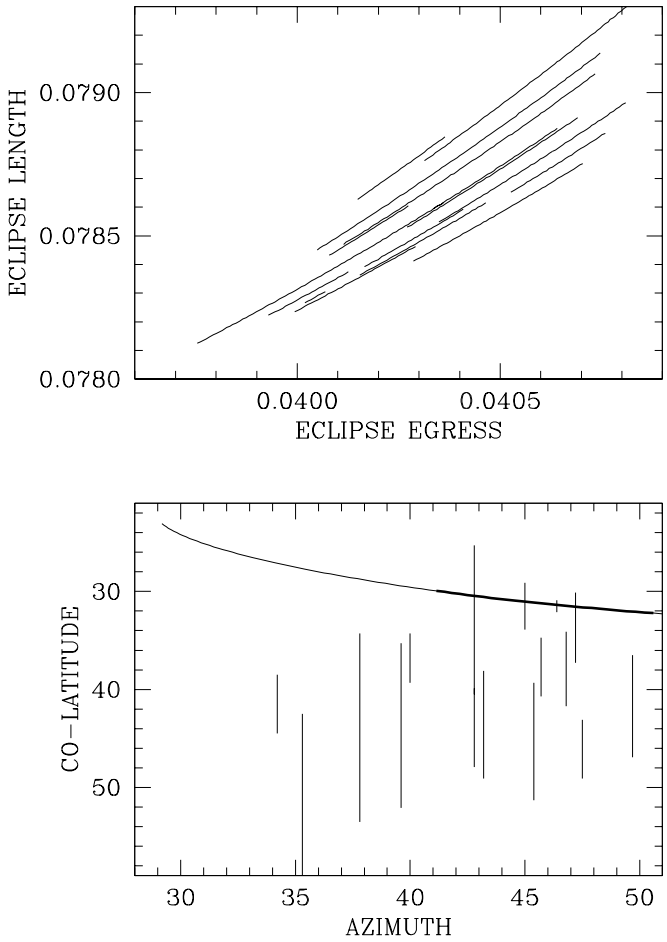

Fig. 6. Light-curve modeling of points on the white dwarf surface. Each line represents one observed eclipse. Azimuth (longitude) and phase of eclipse egress were used as input parameters, the latter with the error as listed in Table 4, eclipse length and lo-latitude are predicted by the model. A phase difference of 0.005 corresponds to 3.75 s. In the upper panel, the azimuth of the point in concern increases from top to bottom. The length of each of the lines shown in the two panels is defined by the measurement uncertainty of the eclipse egress. In the lower panel, the solid line represents the foot-line (accretion arc) of dipolar field lines connecting to the ballistic stream. The bold part of that line corresponds to the observed width of the narrow stream dip.

stars in clusters with spectral type later than M0 above the canonical saturation level of −3. Our results suggest that is true also for the dM5 secondary in HU Aqr.

4.3. Eclipse light curve modeling

The X-ray eclipse of HU Aqr offers an excellent possibility to constrain the size and location of the X-ray emission region on the white dwarf. A very similar system in this respect is UZ For (Warren et al. 1995), in many respects a twin of HU Aqr. We developed a simple but powerful model to reflect the main features of the 1993 PSPC light curve, the only one with sufficient count rate for a detailed eclipse study, under the following assumptions:

– The eclipse ingress and egress are not affected by the PSPC wire mesh. A wire crossing could result in a delayed egress (early ingress) by up to 15 s which is not observed.

– The mass ratio is $Q = M_1/M_2 = 4$ and the orbital inclination $i = 85.6°$. These values are based on high-resolution optical spectroscopy, where the velocity of the secondary star could be measured (Schwope et al. 1997 and unpublished data) and the shape and length of the eclipse in the ultraviolet as seen with the HST/FOS (Schwope et al., in preparation). The lower limit to Q is 3.5 and we made sure that none of the conclusions drawn depends critically on the assumed value of Q.

– The secondary star has a mass $0.17\,M_\odot$, according to the mass-radius relation by Neece (1984). Using the relation by Caillault & Patterson (1990) the mass is $M_2 = 0.15\,M_\odot$. The influence on the fits to the light curve, higher mass M_2 means higher higher mass M_1 means smaller radius $R_{\rm wd}$, is non-negligible but small and will be discussed below.

– The emission region is a circular spot at some height h (in units of the white dwarf radius) above the photosphere. The vertical surfaces of the cylinder do not contribute X-ray flux in our model. This assumption means, that we are able to correctly predict contact points but do not pay very much attention to reflect exactly the shape of the light curve. The spot is divided in small elements, each with the same height. The emission of any visible element at a given phase is either completely optically thin or thick, i.e. the model light curve is the summed visibility function of the surface elements with or without a foreshortening factor.

– The spot has a certain orientation in the binary system defined by the azimuth (longitude) χ, measured with respect to the line joining both stars, and the co-latitude δ, measured with respect to the rotation axis. The azimuth is determined accurately by the phasing of the bright phase centre, $\chi = 46.1° \pm 0.5°$. This value is in agreement with earlier measurements based on optical photometry (e.g. Schwope et al. 1993; Glenn et al. 1994; Harrop-Allin et al. 1999), but here determined with much higher accuracy due to the absence of contaminating radiation from elsewhere in the system.

In X-rays we are seeing the eclipse of a small hot region on the surface of the white dwarf, i.e. away from the centre of mass. A certain phase relation exists between the eclipse of the spot and the eclipse of centre of mass depending on the co-latitude of the spot and the radius of the white dwarf. The height of the emission does not play a role here, since we are seeing the spot projected onto the surface. The mentioned relation is the lever arm to determine the co-latitude of the spot within the limits set by the uncertainty of $R_{\rm wd}$.

The main results of the observations and our modeling are:

– The eclipse lasts 587.5 s in "P Nov. 93". We note, however, that the duration of ingress phase and the exact

start of the phase of totality is somewhat uncertain due to absorption of X-rays in the accretion curtain. The duration of eclipse egress is 1.3 ± 0.3 s. The uncertainty in this quantity derives mainly from the presence of strong flaring outside the eclipse which makes a distinction between geometric and intrinsic variability difficult. The eclipse of the centre of the accretion spot occurs 0.00088 phase units = 6.6 s later than the eclipse of the centre of mass.

– Our model gives best agreement with the observations for a spot size of 3° (full opening angle, see Fig. 5). The maximum possible extent is 4°. This result is not dependent on the assumed height, the co-latitude, or the emission model (optical thick or thin emission). The measured spot size of the assumed circular accretion spot gives a fractional emitting area of the spot of $0.013\,A_{\rm wd}$. The linear dimension across the spot is about 450 km.

– A model without vertical extent (dashed lines in Fig. 5) reproduces the observed rise to and fall from the bright phase. Such a model requires an extreme 'northern' location of the spot at a co-latitude of only 9°. At this high latitude the predicted phase offset between spot centre and centre of mass is much smaller than observed. In order to reproduce the observed length of the bright phase together with the observed phase relation between eclipses of the spot and the centre of mass a more "southern" latitude and a vertical extent of the X-ray emitting region have to be assumed.

– The box-shaped solid line in Fig. 5 (lower left and top panels) represents an optically thin model for an emission region at a height of $0.015\,R_{\rm wd}$ and a co-latitude of 31°. It reflects well the phase relation between centre bright phase, eclipse centre and eclipse length. The statistical uncertainty of the co-latitude is of the order 2°, there is however a somewhat larger systematical uncertainty which is related to the unknown mass of the secondary star. If we, for instance, use the Caillault & Patterson (1990) mass-radius relation for the secondary, the secondary becomes less massive and, for fixed mass ratio, the white dwarf, too. The corresponding larger white dwarf radius results in a different spot position at a co-latitude of 26° in order to get all the phase relations and the eclipse length correct.

– The optically thin model reflects the contact phases well (at eclipse ingress/egress and start/end of the bright phase) and thus constrains the vertical and lateral extent of the emission region. Due to its simplicity, it cannot reproduce the exact shape of the light curve at start and end of the bright phase. In order to cope with this shortcome of the model, we also applied the model presented in Sirk & Howell (1998) to the data, which accounts for a full 3D structure of the emission region. Application of this model for fixed Q, χ and i reveals a spot radius (lateral extent) of 0.0465 $R_{\rm wd}$ (2.7°) and a spot height of 0.0142 $R_{\rm wd}$. These numbers are well in agreement with those derived from the simple 2D model. The fit to the data, however, is clearly much better than that of the 2D model (Fig. 5, bottom right), at least at start and end of the bright phase. This model predicts a maximum count rate of $80\,{\rm s}^{-1}$ in the centre of the bright phase, which is not observed. This deviation is further addressed in Sect. 6. Detailed modeling of the eclipse, however, is not possible with the current version of the 3D code, we therefore use here for the analysis of the eclipse a combination of both models.

– If the assumption of a linear ephemeris (Eq. (1)) is correct and if the white dwarf rotates synchronously, the observed scatter of eclipse egress times must have a geometrical explanation. Both, shifts in longitude (azimuth) and latitude are possible. Azimuthal shifts are obvious from the phase shift $\phi_{\rm CB}$ of the bright-phase centre. According to the values of $\phi_{\rm CB}$ listed in Table 3, the azimuth of the spot varies between ∼35° and ∼50°.

In order to explore the likely size of an latitudinal shift of the accretion hot spot we performed model calculations using our 2D model applied to points on the white dwarf surface. For a given geometry, a point on the white dwarf surface (characterized by its latitude and longitude) has a certain eclipse ingress, eclipse egress, i.e. eclipse length. Observationally, the phase of eclipse egress and the azimuth of the spot can be directly determined. The eclipse model then makes predictions for the remaining parameters, the co-latitude of the spot and the eclipse length. These are plotted for the individual observations in Fig. 6. Each line in the two panels represents one particular observation. The length of each line is determined by the measurement uncertainty of eclipse egress. The uncertainty of the azimuth is almost negligible and was set to zero.

Relevant in Fig. 6 are not the absolute numbers but the range of predicted variability of the co-latitude and the eclipse length. The absolute numbers depend on the radius, hence mass, of the white dwarf, and are therefore somewhat uncertain. From Fig. 6 we obtain, that the co-latitude of the spot likely undergoes shifts as large as ∼15°, similarly to the shift in azimuth. The present data are insufficient to uncover any clear relation between spot longitude and latitude. We can state, however, that the derived locations of surface elements do not stretch along the expected position of an accretion arc, defined as foot-points of dipolar field lines connecting the white dwarf with the ballistic stream for our most likely orientation of the magnetic axis.

According to Fig. 6 variations of the eclipse length of up to ∼8 s ($\Delta\phi = 0.001$) can be expected. This is of the same order as the observed scatter of eclipse egress times. The predicted scatter of the eclipse length can not be confirmed so far with our existing soft X-ray observations. These should be easily detectable with hard X-ray observations using e.g. XMM-Newton, which resolve the eclipse ingress clearly.

5. Spectral analysis

A spectral analysis was performed for the high-state observation referred to as "P Oct. 93". With the resolution provided by the ROSAT-PSPC two spectral components can be discerned clearly, a soft quasi-blackbody component

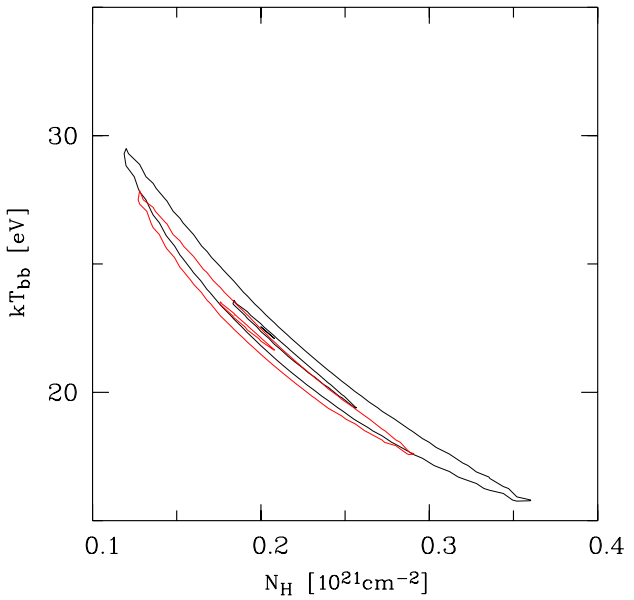

Fig. 7. Results of combined blackbody and bremsstrahlung fits to the "P Oct. 93" observations. Shown are 68% and 99.9% contours for the two phase intervals 0.75−0.83 (slightly harder spectrum with higher temperature and larger column density) and 0.04−0.16, respectively, in the $(N_{\rm H}, kT_{\rm bb})$-plane.

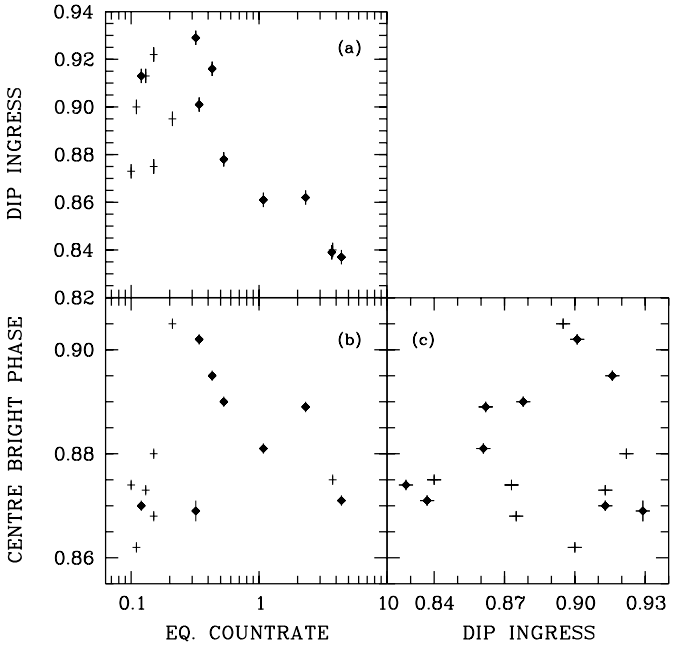

Fig. 8. Relation between (a) equivalent HRI count rate SCR_1 (see Table 3) and phase of dip ingress, (b) equivalent HRI count rate and centre of bright phase, and (c) phase relation between dip ingress and centre of bright phase. Filled rhombs indicate ROSAT-data, crosses indicate EUVE-data.

from the heated photosphere in and around the accretion region and a hard component well described by thermal bremsstrahlung from the hot post-shock region. The temperature of the latter cannot be independently determined with the ROSAT data, since the PSPC does not provide sufficient wavelength coverage. We fixed it at 20 keV. A grid of least-squares fits assuming the two-component model (`bbdy + thbr`) with interstellar cold absorption was performed for two selected phase intervals, for the bright phase prior to the narrow absorption dip, $\phi = 0.75{-}0.83$, and for the post-eclipse bright part of the light curve, $\phi = 0.04{-}0.16$.

The results are shown as confidence contours in Fig. 7. The somewhat softer spectrum at slightly lower $N_{\rm H}$ is observed after eclipse, i.e. the centre of the bright phase phase could be affected by a small amount of extra (intrinsic) absorption. We regard the post-eclipse spectrum as reference for further modeling of the accretion curtain (next section). The best-fit parameters are $N_{\rm H} = 2 \times 10^{20}\,\mathrm{cm}^{-2}$ and $kT_{\rm bb} = 22\,\mathrm{eV}$ ($T_{\rm bb} = 255\,000\,\mathrm{K}$). In the ROSAT band (0.1−2.4 keV) the total un-absorbed blackbody flux is $f_{\rm bb} = 1.39 \times 10^{-9}\,\mathrm{erg\ cm^{-2}\ s^{-1}}$, the total un-absorbed bremsstrahlung flux is $f_{\rm br} = 1.2 \times 10^{-12}\,\mathrm{erg\ cm^{-2}\ s^{-1}}$. The bolometric correction factors for the blackbody and bremsstrahlung components are about 3.2 and 4.6, respectively, i.e. the ratio of the un-absorbed bolometric fluxes is $f_{\rm b,bb}/f_{\rm b,br} = 4.4 \times 10^{-9}/5.4 \times 10^{-12} \simeq 800$. Even taking into account an uncertainty of a factor 2 in both components due to the unknown emission characteristic, the soft excess easily exceeds a factor 100.

Taking into account only the blackbody component, the accretion luminosity and the total accretion rate can be estimated from the spectral parameters or the observed flux at Earth. Assuming a flat circular accretion spot of diameter 450 km and $kT_{\rm bb} = 22\,\mathrm{eV}$, the accretion luminosity is $L_{\rm acc} = \pi r^2 \sigma T_{\rm bb}^4 = 4 \times 10^{32}\,\mathrm{erg\ s^{-1}}$.

Using the observed flux at Earth $f_{\rm b,bb}$ radiated into an angle π, the accretion luminosity is $L_{\rm acc} = \pi D^2 f_{\rm b,bb} = 4 \times 10^{33} (D/180\ \mathrm{pc})^2\,\mathrm{erg\ s^{-1}}$. Both estimates are uncertain to at least 50% due to the unknowns in $T_{\rm bb}$, D, and the emission characteristics. The inferred accretion rate is between $(0.6{-}7) \times 10^{-10}\,M_\odot/\mathrm{yr}$, i.e. at the rate expected for a CV with an orbital period of 2 hours.

Using a two-component model spectrum with the best-fit post-eclipse spectral parameters folded through the instrumental response curves of the PSPC and the HRI detectors, respectively, a count conversion PSPC/HRI = 8 was calculated and used for computation of the equivalent HRI count rates listed in Table 3.

6. The narrow and broad dips and the accretion curtain

The phase of narrow dip centre varies between 0.868 to 0.929, the phase of half intensity at dip ingress varies between 0.828 to 0.929 (Cols. 5 and 6 in Table 3), i.e. the azimuth of the threading region varies by about 36°. The centre of the bright phase varies much less by only 0.04 phase units, corresponding to only about 15°. At the same time the X-ray count rate (equivalent HRI count

rate) varies by a factor 40. Here we investigate the systematics in this behavior.

In Fig. 8 we plot the equivalent count rate SCR_1 vs. dip phase, the centre of the bright phase vs. dip phase, and the equivalent count rate vs. the centre of the bright phase. The numbers are listed in Table 3. By plotting these quantities we are testing if the X-ray count rate varies proportional to the mass accretion rate and whether the penetration of the stream into the magnetosphere can be understood in terms of the interplay between ram pressure and magnetic pressure.

If the X-ray count rate would scale proportional to the specific mass accretion rate and to the ram pressure in the ballistic stream, a unique relation between equivalent count rate and dip phase should exist. One also expects, that the accretion spot migrates towards a larger azimuth if the stream couples further downstream onto magnetic field lines. If the magnetic field would be an aligned dipole, spot azimuth and dip azimuth would vary by the same amount.

Figure 8 shows that the expected relations are quite well established for sufficiently high count rate ($SCR_1 > 0.2\,s^{-1}$) which applies to most ROSAT observations (except "H Oct. 96"), and two EUVE observations ("D May 97", and "D Aug. 98" in low and high accretion states, respectively).

At low count rate (most EUVE observations) the relations break down. The reason for the deviating behavior of the 6 low-state observations is unclear. The ROSAT observation "H Oct. 96" does not fit into the simple picture, but the bright phase centre ϕ_{CB} and the phase of dip ingress ϕ_{DH} are similar to those of the quasi-simultaneous EUVE-observation. The count rate SCR_1 differs by a factor of 2, which we attribute to the non-simultaneity of the observation and the high variability of the source. The ROSAT outlier at the lowest count rate is "H Apr. 96". On that occasion the binary showed a highly peculiar light curve (see Fig. 2). It displayed one of the highest HRI count rates observed ever in the centre of the bright phase while one of the lowest count rates SCR_1 shortly after eclipse, thus mimicking a low state. Since the latter quantity is plotted in Fig. 8, this data point apparently seems to be misplaced in that diagram. The ROSAT data therefore suggest clearly, that at higher accretion rate the stream penetrates the magnetosphere more deeply and couples further downstream onto field lines. As a consequence, the spot longitude is shifted away from the secondary star, i.e. ϕ_{CB} becomes larger. The picture is different for the EUVE data, since the centre of the bright phase does not behave as expected but remains at large azimuthal angles, despite early coupling of the main portion of the stream onto magnetic field lines. This may mean, that some matter runs further downstream even in the low accretion state, builds a hot accretion spot at relatively large azimuth, while the matter that couples early does not dominate the soft X-ray radiation.

In Fig. 9 we investigate the conditions in the accretion stream in a basic picture. The upper panel shows a sketch

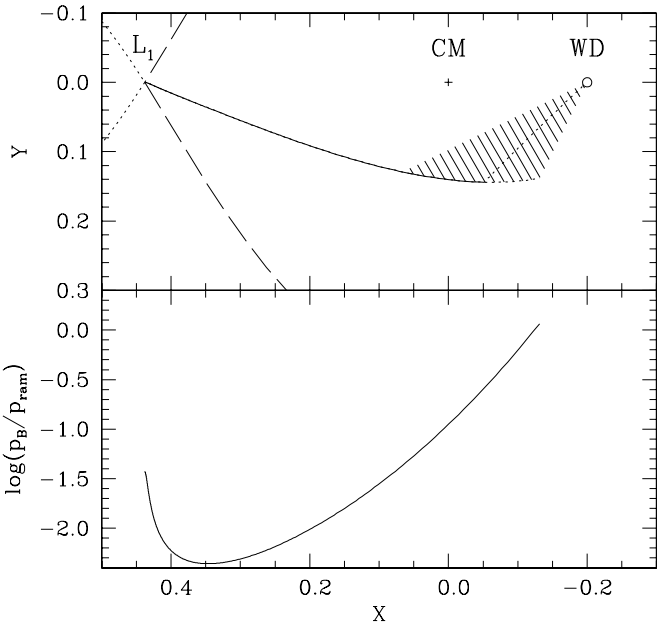

Fig. 9. a), *upper panel)* Stream geometry of HU Aqr projected onto the orbital plane. Indicated are the Roche lobes of both stars, the inner Lagrangian point, the white dwarf and the centre of mass. The shaded region indicates the size of the cone, where dip ingress has been observed (azimuth, where half X-ray intensity occurs, see Table 3). The line in the shaded region connecting the ballistic trajectory and the white dwarf indicates the centroid of the magnetically coupled stream of the "P Oct. 93" observation. **b)**, *lower panel)* The ratio of magnetic and ram pressure along the ballistic stream.

of the accretion geometry projected onto the orbital plane, the lower panel shows the ratio between the magnetic and the ram pressure along the ballistic stream. The trajectory was computed in a single-particle approximation, i.e. neglecting thermal pressure. A mass ratio $Q = M_1/M_2 = 4$, a centred dipole with an inclination of the magnetic axis of 15°, an azimuth of the magnetic axis of 38°, and a polar field strength of 38 MG was assumed. The usage of these parameters results in a spot co-latitude (foot-point of accreting field line) of 31°, in agreement with the observations. The shaded region in the upper panel indicates the observed range of dip ingress phases, according to the 36° variability of ϕ_{DH} as listed in Table 3. The ratio between ram and magnetic pressure varies between these extremes by a factor of ∼27. This number equals the change of the specific mass accretion rate, $\dot{m}$, per unit area. The equivalent HRI count rate varies by a factor of 40. The great similarity between the two numbers suggests that (a) specific and total mass accretion rate scale proportional to each other and that (b) the penetration of the magnetosphere is largely compatible with the simple picture that the location of the coupling region is determined by the balance between ram and magnetic pressure.

We assume that intrinsically the X-ray spectral parameters are constant through the orbital cycle, i.e. that all the X-ray variability in the phase-averaged light curve is due to a differing amount of cold absorbing matter in

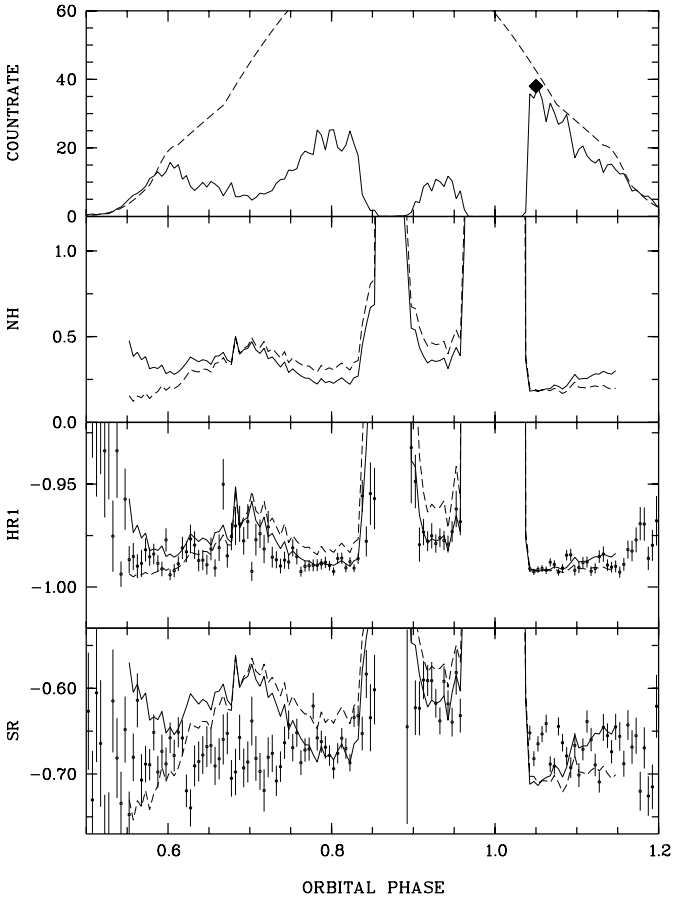

Fig. 10. Soft X-ray brightness, amount of cold absorption, and hardness ratios (HR1 and SR) of HU Aqr in October/November 1993. The phase-folded soft X-ray light curve is shown in the top panel. The map of $N_{\rm H}$ (in units of $10^{21}\,{\rm cm}^{-2}$) in the second panel is based on post-eclipse spectral parameters with respect to constant brightness through the bright phase (solid line) and with respect to the 3D fit (dashed line). In the lower two panels the predictions for HR1 and SR according to the two $N_{\rm H}$-maps are compared with observed data.

the binary system. We then computed a map of $N_{\rm H}$ as a function of orbital phase. This was done under the assumptions of (a) constant X-ray brightness, and (b) of an un-absorbed light curve according to the 3D fit (dotted line in Fig. 5). The spectral parameters and the interstellar absorption were taken from the fit to the post-eclipse data. The results are shown in Fig. 10, together with predicted hardness ratio variations (HR1 and SR) according to the derived value of $N_{\rm H}$. The solid line in each panel is for the constant brightness model, the dashed for the 3D model.

The post-eclipse (interstellar) absorption column density is $N_{\rm H} = 2 \times 10^{20}\,{\rm cm}^{-2}$, in the curtain the column is $N_{\rm H} = 4 \times 10^{20}\,{\rm cm}^{-2}$ and in the narrow dip $N_{\rm H} = (2{-}3){\times}10^{21}\,{\rm cm}^{-2}$. Figure 10 shows that the observed variations of the count rate, the hardness ratios HR1 and SR in the narrow dip and in the curtain, respectively, can be understood in terms of an increase of the column $N_{\rm H}$ of cold absorbing matter. This does not apply to the broad dip at phase 0.7. The predicted increase in $N_{\rm H}$ would result in a decrease of the hardness ratio SR. The occurrence of a broad dip therefore cannot be explained by cold absorption. Either we have a highly complicated surface structure (smaller effective area at phase 0.7 than at phase 0.6), the spectral parameters changed or warm absorption plays a role. The presently available data have too low spectral resolution in order to discern between these alternatives.

Based on the $N_{\rm H}$-map of Fig. 10 we may estimate the accretion rate in the curtain and the stream. Taking the simple view of constant flow velocity $v \simeq 300\,{\rm km\,s}^{-1}$ through the curtain (Schwope et al. 1997) and a length of the curtain given by the length of the ballistic accretion stream, $l = 3{\times}10^{10}\,{\rm cm}$, the mass accretion rate in the curtain is $\dot{M} = \mu m_p N_{\rm H} v l \simeq 4{\times}10^{14}\,{\rm g\,s}^{-1} = 6{\times}10^{-12}\,M_\odot/{\rm yr}$ (μ: mean atomic mass per H-atom). In the dip (= accretion stream), the velocity is higher by a factor $\sim$3, the density higher by a factor of $\sim$10, and the linear dimension is smaller by a factor $\sim$3, i.e. the mass accretion rate in the stream is roughly a factor 10 higher than in the curtain. These order-of-magnitude estimates show, that the amount of matter transfered to the white dwarf via the curtain is clearly non-negligible although the bulk of matter is transfered via the stream. The number derived here for the mass accretion rate, based on the amount of cold absorption, $\dot{M} \simeq 5{\times}10^{15}\,{\rm g\,s}^{-1} = 8{\times}10^{-11}\,M_\odot/{\rm yr}$ is in rough agreement with the estimate based on the X-ray spectral flux (Sect. 5).

We also tested if the observed width of the narrow stream dip and the measured spot size, as derived from the elipse egress, are compatible in a dipolar geometry. The narrow dip has a width of about 18° (phase 0.85–0.90). With our favourite orientation of the dipolar axis, this converges to a spot azimuth along a small circle of about 10°, as indicated in Fig. 6. At a co-latitude of 30° this corresponds to a full opening angle along a great circle of 5°. From the eclipse egress we derived a full opening angle of the soft X-ray emitting spot of 3°−4°. We conclude, that only the inner 60–80% of the stream is dense enough and carries enough accretion energy to "fire" the soft X-ray engine.

7. Summary and conclusions

We have intensively studied the eclipsing polar HU Aqr in soft X-rays using ROSAT and EUVE. During our monitoring observations the source varied in brightness, i.e. mass accretion rate, by a factor of about 40. The one stable feature in the light curves, the eclipse caused by the secondary star, was used to derive an updated linear ephemeris of the binary star. Apparent deviations from a linear trend are likely due to migrations of the accretion spot over the surface of the white dwarf. The implied shifts in spot latitude and azimuth are of the order of 15°.

The eclipse by the secondary star was thoroughly investigated by us. We found X-ray emission in the eclipse

attributed to the secondary star, the implied luminosity of $\sim 2 \times 10^{29}$ erg s^{-1} is comparable to those of single M-stars of same spectral type.

We have successfully modeled the shape, phase, and extent of the soft X-ray eclipse in combination with the phasing and length of the X-ray bright phase in a high accretion state (observation "P Oct. 93"). According to our modeling, the accretion region has a full opening angle of 3°, is located at stellar co-latitude 30°, azimuth 46°, and has a vertical extent of less than $0.015\,R_{\rm wd}$.

An absorption dip caused by the accretion stream passing the line of sight was seen at all epochs. It varied in phase due to changes of the mass accretion rate, hence ram pressure. The observed phase shift of the dip, and of the centre of the bright phase and the observed change of the mass accretion rate can be understood in terms of ram pressure and magnetic pressure balancing arguments. The low-state data, however, most of them obtained with the EUVE satellite, do not fit in this simple picture for an unknown reason.

The X-ray spectrum of HU Aqr, has (at ROSAT resolution) two components, a blackbody-type component with $kT_{\rm bb} = 22\,$eV in the soft regime and a hard bremsstrahlung component with $kT_{\rm br}$ likely to be in the few 10 keV regime. The spectral fit gives a huge soft X-ray excess in the high accretion state of $L_{\rm bb}/L_{\rm br} \sim 800$. The X-ray luminosity derived here, $L_X = 4 \times 10^{32} \ldots 4 \times 10^{33}$ erg s^{-1}, is typical for cataclysmic binaries at an orbital period of 2 hours.

Using the spectral parameters determined in post-eclipse PSPC data, which are supposedly free of internal absorption, we derived the absorption column density in the stream and the accretion curtain. They differ by a factor of ∼10, as do the accretion rates through these structures. These estimates show that transfer of mass along the curtain is non-negligible although insufficient to power significant X-ray emission. In particular, the foot-line of the curtain on the surface of the white dwarf is not bright in X-rays. If it were, the eclipse egress would have taken about 5 s instead of the observed 1.3 s. The accretion energy released at the foot-print of the accretion curtain is not emitted in soft X-rays, but probably shifted to neighbouring spectral regimes (FUV/UV or e.g. as optical cyclotron radiation). The occurrence of a broad dip at binary phase 0.7 cannot be explained by an increase of the column density of cold absorbing matter. Spectral changes when different parts of the accretion region come into view under a different aspect angle or a complicated emitting surface might be responsible for the dip.

X-rays are also detected in the faint phase, when the main accretion spot is out of view. It appears unlikely to us, that this is due to a second accretion spot, since neither optical eclipse light curves nor the optical spectrum in the faint phase show any sign of a second accretion spot, e.g. cyclotron harmonics as seen from the second pole in UZ For (Schwope et al. 1990). Rather than emission from a second pole scattered light from the main pole seems the likely cause of the faint-phase emission.

Further X-ray observations with a larger telescope and higher spectral resolution are necessary in order to gain a better understanding of the spectral composition of this system in general, and of the broad dip in the light curve in particular. Future Chandra or XMM-Newton observations will allow for the first time to measure the accretion spot size in hard X-rays and to investigate whether the predicted variations of the eclipse length occur, they will allow to determine the eclipse spectrum, and to search for X-rays from the accretion stream/stagnation region in the first part of the eclipse by the secondary star.

Acknowledgements. We thank K. Reinsch for providing the optical light curve of Nov. 12, 1995. We gratefully acknowledge the work of our referee, Dr. D. A. H. Buckley.

This work was supported by the DLR-Verbundforschung under grant 50 OR 9706 8. We have made use of the ROSAT Data Archive of the Max-Planck-Institut für extraterrestrische Physik (MPE) at Garching, Germany.

SBH acknowledges partial support of this research from NASA grant NAG5-8644 and by a AO7 EUVE mini-grant.

References

Bowyer, S., Lampton, M., Lewis, J., et al. 1996, ApJS, 102, 129
Buckley, D. A. H., Barrett, P., Haberl, F., & Sekiguchi, K. 1998, MNRAS, 299, 998
Caillault, J.–P., & Patterson, J. 1990, AJ, 100, 825
Glenn, J., Howell, S. B., Schmidt, G. D., et al. 1994, ApJ, 424, 967
Hakala, P. J., Watson, M. G., Vilhu, et al. 1993, MNRAS, 263, 61
Hakala, P. J. 1995, A&A, 296, 164
Harrop-Allin, M. K., Cropper, M., Hakala, P. J., Hellier, C., & Ramseyer, T. 1999, MNRAS, 308, 807
Neece, G. D. 1984, ApJ, 277, 738
Prosser, C. P., Randich, S., & Simon, T. 1998, Astron. Nachr., 319, 215
Prosser, C. P., Randich, S., Stauffer, J. R., Schmitt, J. H. M. M., & Simon, T. 1996, AJ, 112, 1570
Schmitt, J. H. M. M. 1994, ApJS, 90, 735
Schwope, A. D. 1995, Rev. Mod. Astron., 8., 125
Schwope, A. D. 1996, in Cataclysmic Variables and Related Objects, ed. A. Evans, & J. H. Wood (Kluwer), 189
Schwope, A. D., Beuermann, K., & Thomas, H.-C. 1990, A&A, 230, 120
Schwope, A. D., Beuermann, K., & Thomas, H.-C. 1993, A&A, 271, L25
Schwope, A. D., Mantel, K.-H., & Horne, K. 1997, A&A, 319, 894
Schwope, A. D., Beuermann, K., Buckley, D. A. H., et al. 1998, ASP Conf. Ser., 137, 44
Sirk, M. M., & Howell, S. B. 1998, ApJ, 506, 824
Sohl, K. B., Watson, M. G., & Rosen, S. R. 1996, ASP Conf. Ser., 85, 306
Sohl, K. B. 1997, Ph.D. Thesis, Univ. Leicester
Voges, W., Aschenbach, B., Boller, Th., et al. 1999, A&A, 349, 389
Vrielmann, S., & Schwope, A. D. 2001, MNRAS, in press
Warren, J. K., Sirk, M. M., & Vallerga, J. V. 1995, ApJ, 445, 909
Zimmermann, H. U., Becker, W., Belloni, T., et al. 1994, MPE report, 257